Chemical Engineering Journal 475 (2023) 146294

Contents lists available at ScienceDirect

Chemical Engineering Journal

journal homepage: www.elsevier.com/locate/cej

Insights into the surface Structure-Sensitive photocatalytic oxidation of gaseous toluene on Pd/TiO_2 catalysts

Cong Wu [a,1], Qinglong Liu [a,1], Yu Zhan [a], Wei Tan [a], Xiaoqian Wei [a], Qing Tong [b], Haiqin Wan [a,*], Lin Dong [a]

[a] State Key Laboratory of Pollution Control and Resource Reuse, School of Environment, Jiangsu Key Laboratory of Vehicle Emissions Control, Nanjing University, Nanjing 210023, PR China

[b] Jiangsu Key Laboratory of Vehicle Emissions Control, Center of Modern Analysis, Nanjing University, Nanjing 210023, PR China

ARTICLE INFO

Keywords:
Photocatalytic oxidation of gas toluene
Pd/TiO_2 catalysts
Surface oxygen defects
Ti^{3+}
Pd-TiO_2 interaction

ABSTRACT

Indoor volatile organic compounds (VOCs), represented by toluene, can pose a serious threat to human health. In this work, a series of Pd/TiO_2 catalysts with different surface structures (*i.e.*, dispersion/valence of Pd species, surface Ti^{3+}/oxygen defect concentration and Pd-TiO_2 interactions, *etc.*) was constructed by various methods. It was found that the Pd/TiO_2 catalyst prepared by one-step reduction of $NaBH_4$ method (Pd/TiO_2-N) with metallic Pd particles possessed more surface Ti^{3+}/oxygen defects and stronger Pd-TiO_2 interaction than Pd/TiO_2 catalysts prepared by ethylene glycol reduction loading method (Pd/TiO_2-E) and incipient wetness impregnation method (Pd/TiO_2-I). Further photochemical characterizations and reaction mechanism study revealed that the relatively higher concentration of Pd^0 species on Pd particles, stronger Pd-TiO_2 interaction, and more surface Ti^{3+}/oxygen defects on Pd/TiO_2-N could facilitate the generation of more reactive oxygen species (ROS) under light irradiation. The partial oxidation of toluene to benzyl alcohol/benzaldehyde/benzoic acid and the subsequent ring-opening process were found to be highly determined by the valence states of Pd particles and the concentration of surface Ti^{3+}/oxygen defects. This work provides instructive insights into the construction of highly efficient Pd/TiO_2 catalysts for the removal of indoor VOCs.

1. Introduction

Volatile organic substances (VOCs) emitted from furniture, decorations, and building materials could contaminate the indoor environment over prolonged periods and enter the body through various means, such as skin contact, gastrointestinal intake, and respiration inhalation, *etc.*, thus posing serious threats to human health [1–3]. To reduce indoor VOCs, besides improving the quality of raw materials for furniture, decoration, and building construction, and enhancing building ventilation, various strategies (*i.e.*, adsorption, biological purification, low-temperature plasma, and photocatalytic oxidation, *etc.*) have been developed and applied [4–7]. In recent years, photocatalytic oxidation technology has received widespread attention and shown broad application prospects for indoor VOCs treatment for its high efficiency, mild conditions, and non-toxicity [8,9]. An efficient photocatalyst is the key to photocatalytic oxidation technology.

Titanium dioxide (TiO_2) has been widely used as a photocatalyst directly or an important component of a photocatalyst for the oxidation or degradation of air pollutants due to its abundant natural resources, superior chemical stability, low cost and unique photochemical properties [10–12]. A typical photocatalytic process on TiO_2 is initiated by UV-light, which results in the generation of hole-electron (h^-/e^+) pairs and the subsequent separation of electrons and holes. These photogenerated holes can then react with adsorbed water or hydroxyl ions to produce active oxygen species, such as the hydroxyl radical (·OH) and superoxide radicals ($\bullet O_2^-$), *etc.*, which could then efficiently react with the adsorbed reactants on TiO_2 [13]. According to the previous literature, it could be concluded that the photocatalytic oxidation activity on TiO_2 was mainly determined by the efficiency of electron-hole pair generation and separation, the formation of active oxygen species on the TiO_2 surface, and the reaction between active oxygen species and organic compounds adsorbed on the surface [14,15]. However, bare TiO_2 still suffered from several drawbacks (*i.e.*, weak visible light absorption, fast recombination of photogenerated carriers, and low

* Corresponding author.
E-mail address: wanhq@nju.edu.cn (H. Wan).
[1] These authors contributed equally to this work.

https://doi.org/10.1016/j.cej.2023.146294
Received 12 July 2023; Received in revised form 8 September 2023; Accepted 24 September 2023
Available online 26 September 2023

mineralization rate, etc.), which restricted its further practical application. As a result, numerous strategies have been proposed to further improve the photocatalytic oxidation performance of TiO_2 [16–19], and modification with metal active sites was considered as the most effective one [20–22]. Generally speaking, the strong interaction between the deposited metal sites and TiO_2 support as well as the oxygen defects generated at the metal-TiO_2 interface could significantly facilitate the adsorption, activation, and transfer of reactive oxygen species, which could then improve the photocatalytic oxidation performance of TiO_2 [23]. For instance, after the loading of Pt nanoparticles and rational regulation of metal-support interaction, the $Ti^{\delta+}$-Vo•-$Pt^{\delta+}$ interface was formed on the surface TiO_2, thus achieving significantly enhanced photocatalytic activity for toluene oxidation [24].

Among those metals widely used for modifying TiO_2 to enhance its photocatalytic performance, palladium (Pd) has attracted intensive attention due to its remarkable capability in activating carbon-hydrogen (C-H) bonds as well as its nature to form strong interaction with TiO_2. For example, Selishchev *et al.* synthesized Pd/TiO_2 catalysts by photodecomposition method, and they found that a significantly enhanced photocatalytic activity towards the benzene oxidation under UV light was achieved on Pd/TiO_2 catalysts compared to bare TiO_2 [25]. Wu *et al.* also demonstrated that the deposition of Pd nanoparticles could enhance the photocatalytic oxidation performance of TiO_2 by removing excessive surface hydroxyl groups (–OH) on TiO_2 and significantly promoting the formation of active oxygen radicals [26]. Although Pd/TiO_2 catalysts have been reported to exhibit satisfactory photocatalytic performance in VOCs elimination [27], to our knowledge, limited work has been focused on fine-tuning states of the supported Pd species (*i.e.*, dispersion and valence state, *etc.*), the concentration of Ti^{3+}/oxygen defects and the strength of Pd-TiO_2 interaction, as well as revealing the effect of surface engineering on the photocatalytic activity and reaction pathway on Pd/TiO_2 catalysts.

Toluene was one of the most common indoor VOCs, and how to realize efficient toluene removal under mild indoor conditions was widely discussed. In a typical photocatalytic oxidation process, toluene would degrade into a variety of intermediate products adsorbed on the catalyst surface, followed by further oxidation and decomposition into CO_2, H_2O, and other byproducts. Although it has been reported that the whole reaction can be roughly divided into three steps: adsorption of toluene, oxidative decomposition of toluene, and desorption of CO_2/O_2 or by-products, with the ring-opening process being the rate-determining step [24,28], the detailed reaction mechanisms and structure–activity relationship remained unclear even on some classic catalyst systems, such as Pd/TiO_2 [29].

Herein, aimed at exploring the sensitivity of photocatalytic toluene oxidation reaction to the surface structure of Pd/TiO_2 catalysts, Pd/TiO_2 catalysts with different surface structures, including Pd states, surface Ti^{3+}/oxygen defect concentration and the strength of Pd-TiO_2 interaction, were prepared by various synthesis routes and applied for the photocatalytic oxidation of toluene oxidation. Afterward, systematic characterizations were employed to determine the optimal surface structure of the Pd/TiO_2 catalyst, reveal the reaction mechanisms, and establish a clear structure–activity relationship in the photocatalytic oxidation of toluene. This work will try to fill the gap in the understanding of the surface structure-sensitive photocatalytic oxidation of toluene on Pd/TiO_2 catalysts.

2. Experimental section

2.1. Catalyst preparation

Anatase TiO_2 was obtained from Aladdin Reagent Company. To remove surface impurities, the anatase TiO_2 was calcined in a muffle furnace at 400 °C for 4 h before use.

Pd/TiO_2 catalysts with a theoretical Pd loading of 1 wt% were prepared by sodium borohydride one-step reduction method, glycol reduction loading method, or incipient wetness impregnation method.

2.1.1. Pd/TiO_2 catalyst prepared by one-step reduction of sodium borohydride method

Firstly, 40 mg $NaBH_4$ was dissolved in 10 mL of deionized water and stirred in an ice water bath for 20 min. A certain amount of Na_2PdCl_4 was weighed in 20 mL of deionized water and stirred, and after adding 1.0 g of TiO_2 powder, $NaBH_4$ was added dropwise using a peristaltic pump at a speed of 6 rpm. The sample was then washed by centrifugation with deionized water and transferred to an oven for drying at 80 °C for 12 h. The obtained sample was labeled as Pd/TiO_2-N.

2.1.2. Pd/TiO_2 catalyst prepared by ethylene glycol reduction loading method

Firstly, 15 mL ethylene glycol was placed in a 50 mL three-neck flask and 20 mg PVP was added and mixed well. The microwave reactor was heated to 150 °C and stabilized for 5 min. 1.2 mL Na_2PdCl_4 ethylene glycol solution was added dropwise, followed by the rapid addition of 1 mL NaOH (0.25 M). After the mixture reacted at 150 °C for 30 min, the three-neck flask was immediately immersed in an ice-water bath for 30 min, and the resulting solution was dispersed in a centrifuge tube and washed and centrifuged by adding excess acetone to settle down the Pd nanoparticles. After pouring off the supernatant, 5 mL of ethanol was added to each centrifuge tube separately, sonicated for 5 min to enable uniform dispersion, and then hexane was added for centrifugation, and the operation was repeated twice to remove PVP. The final product was dispersed in an ethanol solution, dropped into a mixture of TiO_2 and ethanol, stirred for 2 h and then evaporated in a water bath, and then dried at 80 °C for 12 h. The resulting sample was labeled as Pd/ TiO_2-E.

2.1.3. Pd/TiO_2 catalyst prepared by incipient wetness impregnation method

1 g of TiO_2 powder was pre-dried in an oven, an appropriate amount of Na_2PdCl_4 was dissolved in deionized water, and the solution was added dropwise to the carrier in batches of 100 μL. To ensure uniform impregnation, a glass rod was used for continuous stirring during the dropwise addition to keep the powder in a lump-free state. After impregnation, the samples were dried in an oven at 80 °C for 12 h and then calcined in a muffle furnace at 400 °C for 4 h. The resulting samples were labeled as Pd/TiO_2-I.

2.2. Catalytic performance evaluation

Before the reaction, the catalyst was purged with air at a flow rate of 50 $mL{\cdot}min^{-1}$ for 40 min. The catalytic performance of the prepared catalysts in photocatalytic oxidation of toluene was evaluated on a continuous-flow stainless steel reactor equipped with a quartz opening window on the top under the 280 W Xe lamp irradiation. In each test, 50 mg of the sample was evenly dispersed on a 400-mesh screen and placed in the reactor. The toluene concentration was stabilized at 50 ppm by diluting the 200-ppm toluene/Airflow with high-purity air (20 vol% O_2/N_2). At the same time, the relative humidity (RH) of the feeding stream was controlled at *ca.* 55 % using a bubbling method. After reaching an equilibrium of toluene absorption and desorption under dark conditions, the photocatalytic oxidation of toluene was started under irradiation by a 300 W Xenon lamp. The concentration of toluene and CO_2 in the outlet gas was monitored by gas chromatography (GC-7920). The formulas used to calculate the toluene conversion and mineralization rate were as follows:

$$\text{Toluene conversion } (\%) = \frac{[\text{Toluene}]_{in} - [\text{Toluene}]_{out}}{[\text{Toluene}]_{in}} \times 100\%$$

$$\text{Toluene mineralization } (\%) = \frac{[CO_2]_{out}}{7 \times [\text{Toluene}]_{in}} \times 100\%$$

where $[\text{Toluene}]_{in}$ and $[\text{Toluene}]_{out}$ are the concentration (ppm) of

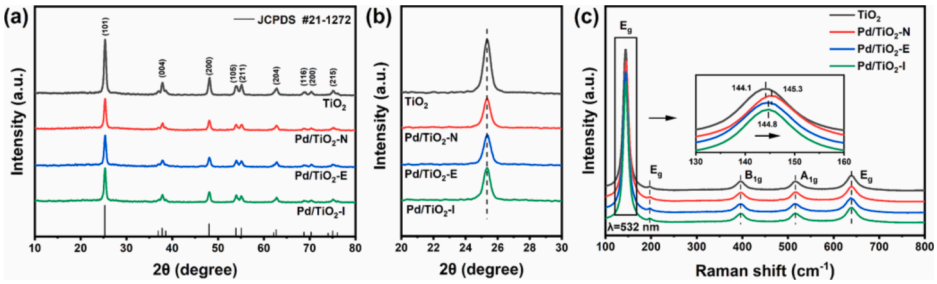

Fig. 1. **(a)** The full XRD patterns, **(b)** the partial magnification of XRD patterns (20° −30°) and **(c)** Raman spectra of TiO_2 and Pd/TiO_2 catalysts.

toluene in the inlet and outlet flow, respectively. $[CO_2]_{out}$ represents the concentration (ppm) of product CO_2 in the outlet flow.

TOF (Turnover Frequency) is calculated using the dispersion of Pd (based on the result of TEM) and the conversion of toluene in Pd/TiO_2 catalysts. The formulas used to calculate TOF values were as follows:

$$TOF = \frac{(\text{Toluene Conversion}) \times 50\text{ppm} \times 0.05\ \text{L/min}}{22.4\ \text{L/mol} \times \frac{m_{Pd}}{195\ \text{g/mol}} \times D_{Pd} \times 60\ \text{s/min}}$$

2.3. Catalysts characterization

XRD patterns were collected using a Philips X'pert Pro diffractometer with a Ni-filtered Cu Kα radiation (λ = 0.15408 nm). The X-ray tube was running at 40 kV and 30 mA, and the 2θ data from 10° to 80° was collected at $10^{\circ}\cdot min^{-1}$.

The surface area of the samples was evaluated at 77 K with N_2 adsorption–desorption isotherms on a Quanta chrome Autosorb-iQ instrument. Prior to testing, all samples were degassed under a vacuum at 200 °C for 2 h. The Brunauer-Emmett-Teller (BET) methods were applied to determine the surface area in the partial pressure range of 0.05 to 0.30.

The Raman of catalysts was collected on the LabRAM spectrophotometer with a resolution 2 cm^{-1}. As the source of excitation, the laser was a 532 nm solid state semiconductor laser with pumped diodes, with an output power of 30 MW.

The ESR analysis was collected on the Brukers EMx spectrophotometer at the frequency 10 $g\cdot h^{-1}$ and with a 100-kHz magnetic field.

Experiments of X-ray photoelectron spectroscopy (XPS) were conducted with the PHI 5000 VersaProbe system, and using monochromatic Kα-rays at an energy of 1486.6 eV with an acceleration rate of 15 kW. Calibration of all binding energies (BE) was done by counterbalancing the charging effects of samples with the adventitious C 1 s peak at 284.6 eV.

Transmission electron microscopy (TEM) and high-resolution TEM (HRTEM) were conducted on a JEM-2100 instrument at an acceleration voltage of 200 kV.

The photoelectrochemical measurements were carried out on a CHI660E electrochemical workstation equipped with a standard three-electrode cell. The photocatalytic sample was applied on fluorine-doped Tin Oxide (FTO) function as the working electrode and the platinum wire electrode and Ag/AgCl electrode were considered as the counter and reference electrodes, respectively, and the test condition was contrasted according to references. Meanwhile, the electrolyte solution was Na_2SO_4 (0.1 M) and the light source was a Xenon arc lamp. In the on–off cycles of illumination, the transient photocurrent response was collected at 0.5 V versus Ag/AgCl.

Photoluminescence (PL) spectra were obtained using an F-7000 fluorescence spectrophotometer with the excitation light of 320 nm wavelength.

In situ-DRIFTS experiments were conducted on a Nicolet Nexus 5700 FTIR spectrometer. Each photocatalyst was pre-treated with purified N_2 for 1.5 h at 200 °C and then cooled to 30 °C for the collection of the sample's background spectra. Thereafter, toluene adsorption DRIFTS was recorded for 40 min with the introduction of 50 ppm toluene/air. *In situ* DRIFTS of photocatalytic toluene experiments were conducted under the illumination of an Xe lamp in a 50-ppm toluene/air atmosphere.

The redox properties of the samples were assessed using temperature-programmed desorption of O_2 (O_2-TPD) conducted with the Micromeritics ASAP 2920 instrument (Micromeritics, USA). Initially, 100 mg of the samples underwent pretreatment at 200 °C with a He flow rate of 50 $mL\cdot min^{-1}$ for 40 min. Subsequent to cooling to room temperature, a flow of 20 % O_2 at 50 $mL\cdot min^{-1}$ was purged for 1 h. Following this, a helium (He) purge at 50 $mL\cdot min^{-1}$ was employed to eliminate physically adsorbed O_2. The O_2-TPD curve was recorded when the baseline was stable, involving the gradual heating of the sample from room temperature to 750 °C at a rate of 10 $°C\cdot min^{-1}$. For the toluene temperature programmed desorption (toluene-TPD), oxygen replaced toluene, while all other experimental conditions remained unaltered.

3. Results and discussion

3.1. Texture property and morphology

To investigate the crystalline structures of TiO_2, Pd/TiO_2-N, Pd/TiO_2-E, and Pd/TiO_2-I catalysts, XRD patterns of them were collected and shown in Fig. 1**a**. The peaks at 25.33°, 37.88°, 48.09°, 54.02°, 55.11°, and 62.79° were in good accordance with the characteristic diffraction peaks of anatase TiO_2 (**JCPDS 21-1272**). No diffraction peak related to the crystalline Pd species was observed on the XRD patterns for all Pd/TiO_2 catalysts. Moreover, no significant shift was observed in the diffraction peak positions of the four samples, suggesting that Pd ions were not doped into the lattice of TiO_2. To further support our viewpoint, the region containing (1 0 1) peak was enlarged for comparison (Fig. 1**b**). It could be observed that no shift of the XRD peaks occurred after the deposition of Pd species. Further calculations using Scheller's formula for the XRD results are shown in Table S1, where the Pd/TiO_2 samples all have approximated half-peak widths and crystallite sizes. More interestingly, the intensity of the TiO_2 diffraction peaks decreased after the loading of Pd species, which could be related to the generation of more surface lattice defects induced by Pd species [30].

Since the catalytic reaction mainly occurred on the surface of the catalysts, Raman spectroscopy was employed to characterize the surface structure of Pd/TiO_2 catalysts. As shown in Fig. 1**c**, typical Raman vibrational peaks for anatase TiO_2 can be clearly observed at 144 cm^{-1}(E_g), 198 cm^{-1}(E_g), 398 cm^{-1} (B_{1g}), 520 cm^{-1} (A_{1g}) and 638 cm^{-1} (E_g) [31]. It was worth noting that a blue shift of the Raman vibrational peak (in the case of the strong E_g near 144 cm^{-1}) occurred after the loading of Pd. According to previous reports, this was due to the strong interaction between the Pd species and TiO_2 support and the formation of oxygen defects at the Pd-TiO_2 interface [18]. The most significant blue shift of Raman peaks on Pd/TiO_2-N indicated the formation of the strongest Pd-TiO_2 interaction and the most abundant oxygen defects.

The catalytic performance of a catalyst is determined by various factors, among which the specific surface area always plays a crucial role

Table 1
The results of N_2 physisorption and ICP experiments.

Samples	Surface area ($m^2 \bullet g^{-1}$)	Pore volume ($cm^3 \bullet g^{-1}$)[a]	Pore size (nm)	Pd loading (%)
TiO_2	68.7	0.30	17.7	–
Pd/TiO_2-N	64.8	0.28	17.5	0.61
Pd/TiO_2-E	62.4	0.28	18.1	0.70
Pd/TiO_2-I	56.7	0.29	20.4	0.67

[a] The specific surface areas of prepared catalysts were measured by N_2 physisorption at −196 °C.

as it determines the contact area between the catalyst and the reactants [15]. In this study, the specific surface areas of the catalysts were measured and listed in Table 1. N_2 adsorption–desorption isotherms and pore size distribution of TiO_2 support and Pd/TiO_2 catalysts were demonstrated in Fig. S1. The specific surface area of the samples before and after Pd loading did show rather limited differences, suggesting that the specific surface area or pore structure would not have a significant impact on the catalytic performance of Pd/TiO_2 catalysts. To confirm the actual loadings of Pd species, ICP-OES analysis was performed. As listed in Table 1, Pd/TiO_2-N (0.61 wt%), Pd/TiO_2-E (0.70 wt%), and Pd/TiO_2-I (0.67 wt%) showed similar Pd loadings.

In addition, the morphologies of the Pd/TiO_2-N, Pd/TiO_2-E, and Pd/TiO_2-I catalysts were investigated using TEM and the results were shown in Fig. 2. For all catalysts, the TiO_2 support showed an average particle size of *ca.* 25 nm and Pd particles were uniformly dispersed on the TiO_2. Pd particle size distribution analysis further revealed that the Pd particles on both Pd/TiO_2-N and Pd/TiO_2-E showed a narrow size distribution and a similar average size of *ca.* 5.7 nm and this is consistent the EDS mapping results of Fig. S2, while the Pd nanoparticles in Pd/TiO_2-I showed a much wider particle size distribution and a smaller average particle size (2.8 nm). High-resolution transmission electron microscopy (HR-TEM) analysis indicated that the lattice spacing of TiO_2 support was 0.35 nm, which was consistent with the value of TiO_2(1 0 1) for anatase TiO_2 [32,33]. Moreover, the lattice spacing of 0.228 nm on Pd/TiO_2-N and Pd/TiO_2-E could be indexed as the (1 1 1) facets of metallic Pd. As for Pd/TiO_2-I, the relatively smaller size of Pd particles made it difficult to determine the exposed facets.

3.2. Photocatalytic performance in toluene oxidation

The photocatalytic performance of Pd/TiO_2 catalysts prepared by various synthesis methods in toluene oxidation was evaluated. As shown in Fig. 3**a**, after the deposition of Pd, the toluene oxidation conversion on TiO_2 increased to varying degrees, and the activity on Pd/TiO_2 prepared by different methods followed an order of Pd/TiO_2-N > Pd/TiO_2-E > Pd/TiO_2-I, suggesting that Pd particles prepared by one-step reduction of sodium borohydride method could better facilitate the photocatalytic oxidation of toluene. All Pd/TiO_2 catalysts exhibited higher mineralization rates than bare anatase TiO_2 (Fig. 3**b**), suggesting that Pd sites played an important role in the deep mineralization of toluene [34]. Moreover, Pd/TiO_2-N exhibited the highest mineralization rate among all Pd/TiO_2 catalysts. Considering that Pd/TiO_2-N with the highest mineralization rate also showed the best stability (Fig. 3**a**) and other catalysts suffered from continuous deactivation with increasing reaction time, it could be proposed that the deactivation of TiO_2, Pd/TiO_2-E, and Pd/TiO_2-I might be related to the accumulation of carbonaceous intermediates on the surface of the catalysts. The more obvious change in the color of TiO_2, Pd/TiO_2-E, and Pd/TiO_2-I after catalytic performance evaluation also well supported our viewpoint [35] (Fig. S3). The stability of Pd/TiO_2-N in photocatalytic oxidation of toluene was further evaluated by a three-round cycling test, and the results were shown in Fig. 3**c**. Only a slight decrease in the toluene conversion was observed on

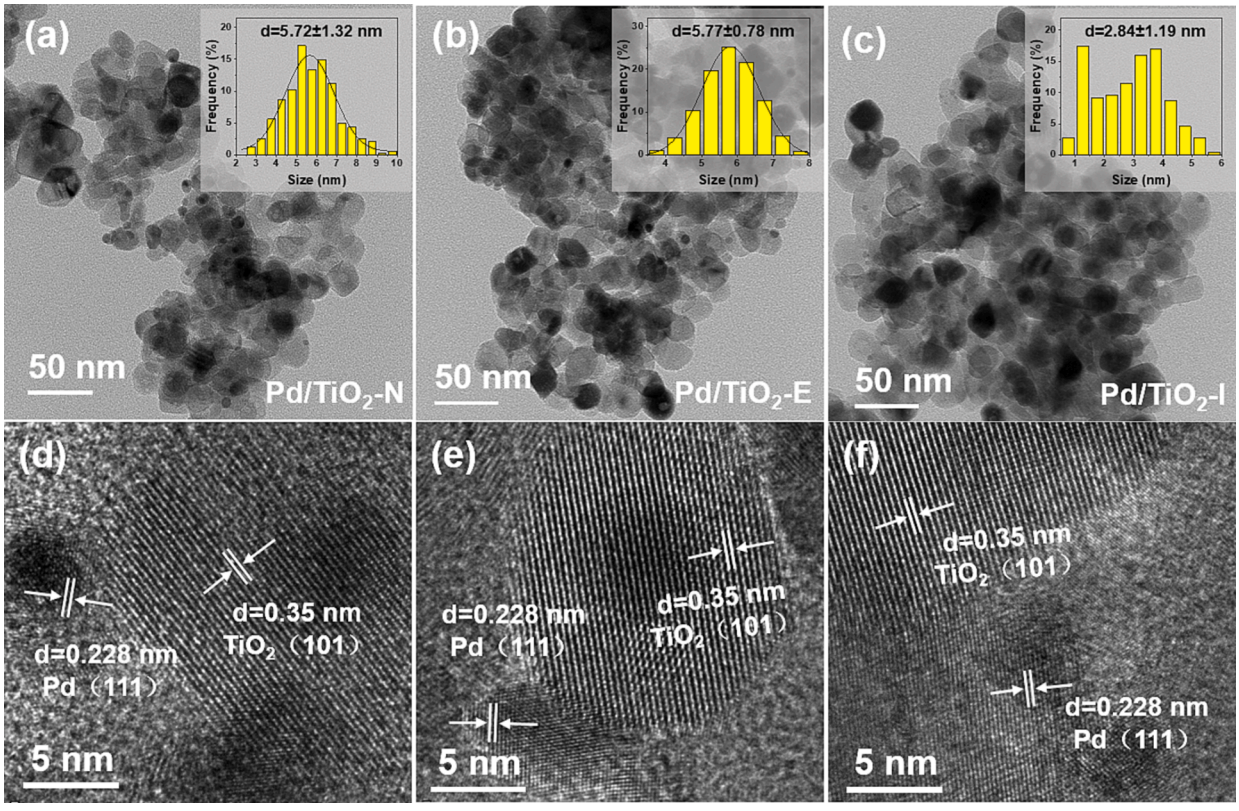

Fig. 2. TEM images and Pd particle size distributions of **(a)** Pd/TiO_2-N; **(b)** Pd/TiO_2-E; **(c)** Pd/TiO_2-I (Note: For each catalyst, more than 500 Pd particles were counted); HR-TEM images of **(d)** Pd/TiO_2-N;**(e)** Pd/TiO_2-E; **(f)** Pd/TiO_2-I.

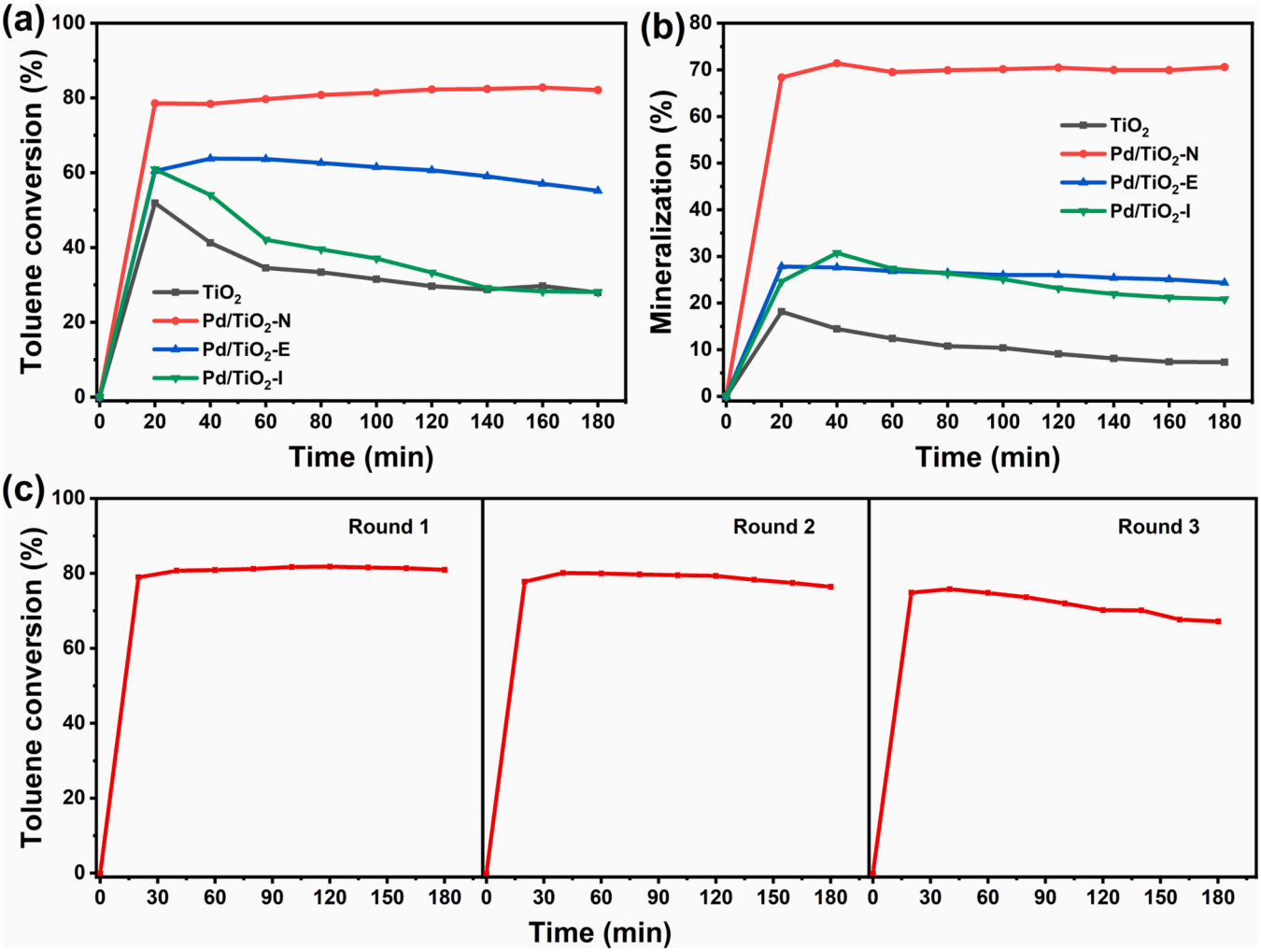

Fig. 3. **(a)** Toluene conversion and **(b)** mineralization rate on TiO_2 and Pd/TiO_2 catalysts in photocatalytic oxidation of toluene. Reaction conditions: [Toluene] = 50 ppm; [O_2] = 20 %, N_2 as balance. **(c)** Cyclic test on Pd/TiO_2-N sample in photocatalytic oxidation of toluene.

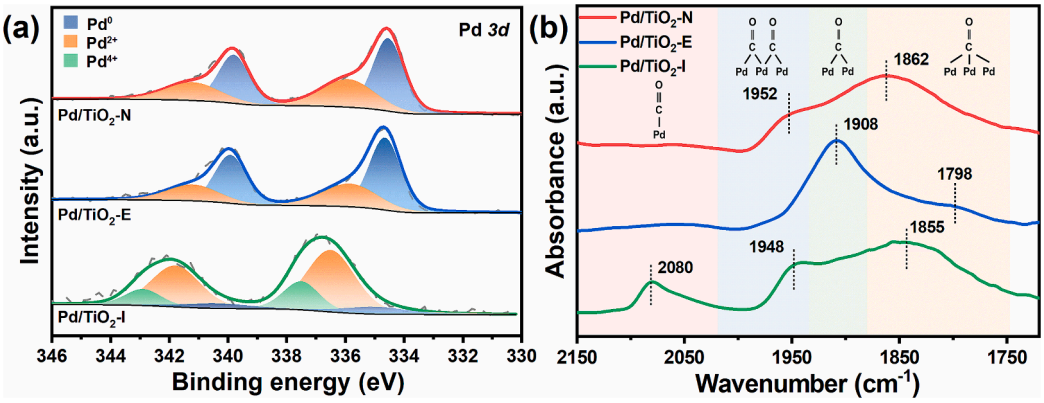

Fig. 4. **(a)** Pd 3d XPS for Pd/TiO_2 catalysts; **(b)** *in-situ* DRIFTS of CO adsorption on the Pd/TiO_2 catalysts.

Pd/TiO_2-N in the three-round cycling test, suggesting its superior stability. The results from the TOF values also demonstrate that Pd/TiO_2-N had the highest frequency of catalytically active sites involved in the reaction per unit time (Fig. S4).

Inspired by the results of Raman spectroscopy that stronger Pd-TiO_2 interaction and more surface oxygen defects were formed on Pd/TiO_2-N, the states of Pd species, the strength of Pd-TiO_2 interaction and the concentration of surface oxygen defects at Pd-TiO_2 interface might greatly determine the adsorption and activation of toluene as well as the further conversion and desorption of intermediates. To confirm this hypothesis, more detailed characterizations and further discussions were carried out in the following section.

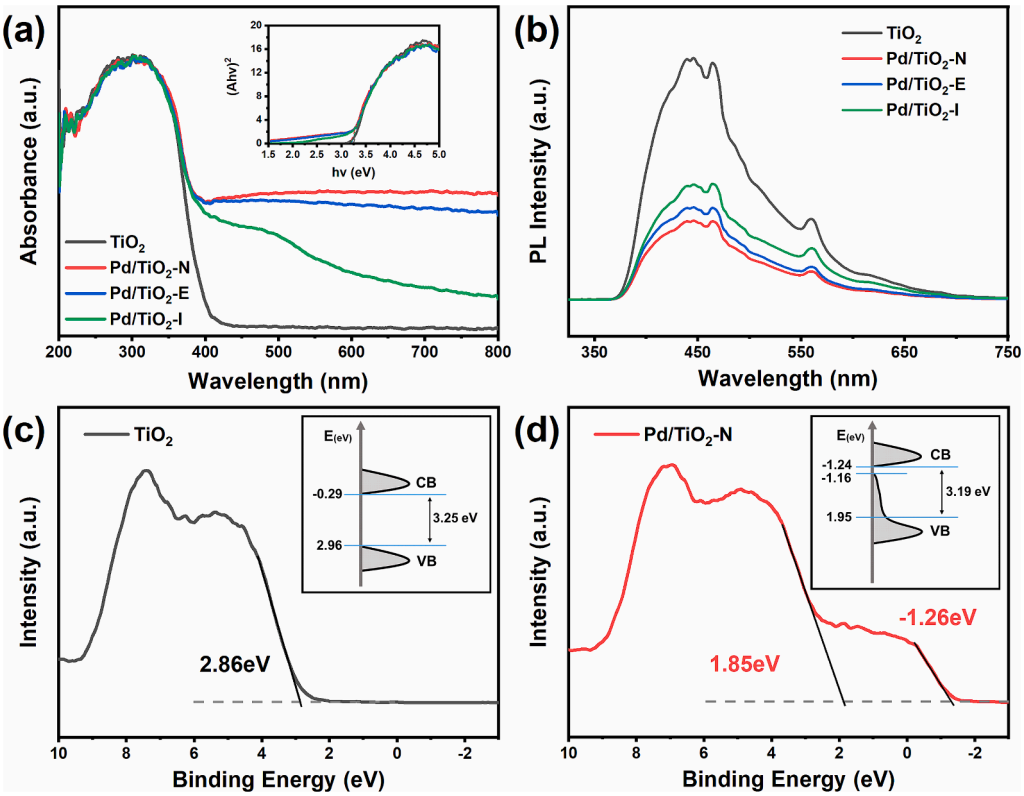

Fig. 5. **(a)** UV–vis DRS spectra and **(b)** PL spectra for Pd/TiO_2 catalysts. VB XPS spectra and proposed schematic energy band structure for **(c)** TiO_2 and **(d)** Pd/TiO_2-N.

3.3. Pd state and photoelectrochemical properties

XPS and *in-situ* DRIFTS of CO adsorption experiments were employed to investigate the dispersion and the chemical states of Pd species on Pd/TiO_2 catalysts synthesized by different methods.

Pd 3d XPS spectra for Pd/TiO_2 catalysts were collected and presented in Fig. 4**a**. XPS peaks assigned to Pd^0 (335.5 and 341.5 eV), Pd^{2+} (336.3 and 342.9 eV) and Pd^{4+} (337.3 and 343.9 eV) species were marked in blue, orange and green, respectively, and the ratio of Pd species in different valence states was further calculated and listed in Table S2. It was revealed that the Pd species on Pd/TiO_2-I predominantly existed in the form of oxidized Pd species (Pd^{2+} and Pd^{4+}, 90.3 %), while Pd species on both Pd/TiO_2-N and Pd/TiO_2-E were mainly in the form of Pd^{2+} (*ca.* 40 %) and metallic Pd (*ca.* 60 %).

As a supplement to XPS experiments, *in-situ* DRIFTS of CO adsorption were conducted to further determine the dispersion and chemical states of Pd species [36,37]. As shown in Fig. 4**b**, several distinctive bands were observed on all catalysts after the exposure to CO flow and further N_2 purging. The band at *ca.* 2080 cm^{-1} was assigned to linearly adsorbed CO on ionic Pd single sites in PdO_x structure (CO-$Pd^{\delta+}$@PdO_x), while those bands at 1930–2020 cm^{-1}, 1880–1930 cm^{-1} and 1750–1880 cm^{-1} were assigned to the collective oscillation of CO on metallic Pd clusters (CO-Pd^0). Since the CO-$Pd^{\delta+}$@PdO_x band was absent on Pd/TiO_2-E and Pd/TiO_2-N, it could be speculated that $Pd^{\delta+}$ sites on the surface of Pd particles on both Pd/TiO_2-E and Pd/TiO_2-N could be easily reduced to Pd^0 in CO flow. However, for Pd/TiO_2-I, abundant PdO_x particles on it were less reducible, thus generating an intensive CO-$Pd^{\delta+}$@PdO_x band. When combined with the results of HR-TEM and Pd 3d XPS, it could be concluded that the aggregated Pd species on Pd/TiO_2-N and Pd/TiO_2-E should be in the form of metallic Pd particles partially covered by PdO_x species, while the aggregated Pd species on Pd/TiO_2-I mainly existed in the form of PdO_x particles.

As reported previously, $Pd^{\delta+}$ could better favor the activation of C-H bonds in organic compounds [38,39], while Pd^0 could benefit the enrichment of electrons on the catalyst surface and enhance the electron-hole separation efficiency [40,41]. The more efficient utilization of photogenerated carriers on Pd^0-TiO_2 catalysts could better facilitate photocatalytic reactions. Although the high concentration of $Pd^{\delta+}$ on Pd/TiO_2-I could efficiently activate the C-H bonds in toluene, the lack of Pd^0 species would result in the inefficient further degradation of intermediates and thus the accumulation of carbonaceous species, well explaining the rapid deactivation of Pd/TiO_2-I in photocatalytic performance evaluation (Fig. 3**a**). In clear contrast, a reasonable ratio of $Pd^{\delta+}$ to Pd^0 (39.8 % *vs.* 60.2 %) on Pd/TiO_2-N could benefit the activation of C-H bonds and further degradation of intermediate species at the same time. As a result, Pd/TiO_2-N exhibited higher toluene conversion and mineralization as well as superior stability.

It has been widely reported that the loaded metal species could modulate the energy band structure and the light absorption properties of TiO_2 [21,42]. To further investigate the photoelectrochemical properties of the prepared Pd/TiO_2 catalysts, UV–vis DRS and valence band XPS (VB-XPS) experiments were carried out.

As shown in Fig. 5**a**, all catalysts show typical TiO_2 UV strong absorption at 250–400 nm. Moreover, after the deposition of Pd onto the TiO_2, a significantly enhanced light absorption in the visible region was observed. The strong absorption at 400–800 nm on Pd/TiO_2-N and Pd/TiO_2-E should be caused by the presence of Pd clusters [43–45], while the obvious absorption broad peak between 450 and 550 nm on Pd/TiO_2-I should be related to the local gap state of PdO_x at the PdO_x/TiO_2 surface caused by the interbond leap of PdO_x [46,47]. The forbidden bandwidths calculated by Tauc plot conversion were shown in Table S3. The band gap of TiO_2 could be narrowed by Pd modification, which could facilitate the absorption of light.

The valence band density of states (DOS) of TiO_2 and Pd/TiO_2 catalysts was determined by VB XPS experiments, as shown in Fig. 5**(c-d)** and Fig. S5. The bare TiO_2 support showed typical TiO_2 valence band

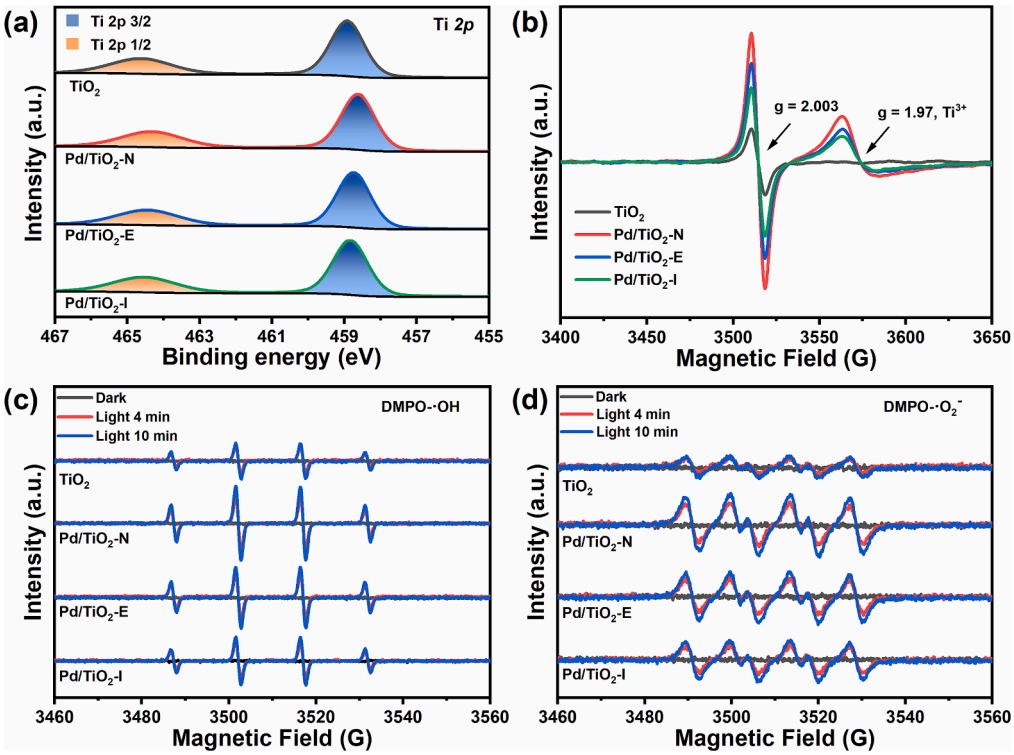

Fig. 6. **(a)** XPS spectra of Ti 2p; **(b)** ESR plots of the O vacancy and Ti^{3+}; ESR spectra under light irradiation for 10 min for **(c)** DMPO-·OH and **(d)** DMPO-·O_2– of Pd/TiO_2-N, Pd/TiO_2-E, Pd/TiO_2-I, and TiO_2.

characteristics with a direct measurement of the valence band maximum (VBM) potential of about 2.86 eV, which was calibrated to 2.96 eV according to a standard hydrogen electrode (NHE) [48]. Also, a sub-occupied energy level was observed in the valence band of the prepared Pd/TiO_2 catalysts, showing an additional valence band tail state, which was not observed in the spectrum of TiO_2. The valence band tails can be resulted from the strong electron absorption of the TiO_2 surface modified with Pd species, which was rich in Ti^{3+} or local lattice defects. These defects introduce an additional diffuse electronic state above the valence band edge, thus resulting in a narrowing of the optical band gap of the Pd/TiO_2 samples via interband transition. The calibrated main valence band energy levels of Pd/TiO_2-N, Pd/TiO_2-E, and Pd/TiO_2-I are 1.95, 2.22, and 2.22 eV, respectively, and the corresponding VBM were −1.16, −0.92, and 0.49 eV. In combination with the results of VB and UV–vis DRS, the calculated conduction band values of the Pd/TiO_2 catalysts are shown in Table S3. It could be concluded that the richest Ti^{3+} on Pd/TiO_2-N resulted in its most negative VBM, which should be one of the main reasons for the superior photocatalytic activity on Pd/TiO_2-N.

PL emission spectroscopy has been widely employed to investigate the charge carrier trapping, migration, and transfer behaviors of semiconductor particles. As illustrated in Fig. 5**d**, the intensity of the PL spectra for TiO_2 and Pd/TiO_2 catalysts followed an order of Pd/TiO_2-N < Pd/TiO_2-E < Pd/TiO_2-I < TiO_2, which should be related to the effective electronic capture of Pd species on the Pd/TiO_2 surface [43,49]. The effectively hindered electron-hole complexation on the Pd/TiO_2-N catalyst would also facilitate the photocatalytic oxidation of toluene.

3.4. Oxygen defects and reactive oxygen species (ROS)

Ti 2p XPS were collected and analyzed to gain a deeper understanding of the chemical states of Ti species. As shown in Fig. 6**a**, the two well-defined peaks ascribed to Ti $2p_{3/2}$ (458.5——458.8 eV) and Ti $2p_{1/2}$ (464.3——464.5 eV) were in good agreement with the characteristic features of TiO_2 [50]. In comparison with TiO_2, the Ti 2p XPS peak of all Pd/TiO_2-I, Pd/TiO_2-E and Pd/TiO_2-N shifted towards lower binding energy, indicating the higher electron density of the Ti atoms in Pd/TiO_2 samples than that in TiO_2, suggesting the formation of Pd-TiO_2 strong interaction and TiO_{2-y} species [51]. Moreover, the higher shift value of Ti $2p_{3/2}$ on Pd/TiO_2-N (0.3 eV) than that on Pd/TiO_2-E (0.2 eV) and Pd/TiO_2-I (0.1 eV) indicated that stronger Pd-TiO_2 interaction, matching well with the results of Raman spectra. At the same time, there might be a higher concentration of surface Ti^{3+}. The presence of Ti^{3+} within the surface lattice of TiO_2 was also accompanied by the formation of oxygen defects, which could play an important role in photocatalytic oxidation reactions [52,53].

Since Ti^{3+} ions with unpaired electrons could be polarized and interact with the magnetic field, the presence of Ti^{3+} ions can be further characterized using ESR. As shown in Fig. 6**b**, the characteristic g values of 2.003 and 1.97 could be assigned to oxygen defects/vacancies (Ov) and Ti^{3+} ions [51,54]. The signal intensity for oxygen defects and Ti^{3+} ions on Pd/TiO_2 catalysts followed an order of Pd/TiO_2-N > Pd/TiO_2-E > Pd/TiO_2-I, well consistent with the findings from XPS analysis that the highest concentration of Ti^{3+} ions and oxygen defects were created on Pd/TiO_2-N. This might be due to the fact that $NaBH_4$ (a strong reducing agent) used in the one-step reduction method can reduce not only Pd species but also TiO_2 support, thus generating more Ti^{3+} and oxygen defects on Pd/TiO_2-N. In contrast, ethylene glycol used in the ethylene glycol reduction loading method could only react with Pd species without further reducing TiO_2 support. Although the Pd particles on Pd/TiO_2-N and Pd/TiO_2-E exhibited similar size as well as oxidation states, the higher concentration of surface Ti^{3+} and oxygen defects on Pd/TiO_2-N well explained its much better performance in photocatalytic oxidation of toluene.

The reactive oxygen species (ROS) played a crucial role in the photocatalytic oxidation of toluene. ESR technique has been widely applied for the detection and qualification of free radicals, including various ROS (*e.g.*, superoxide radicals ($\bullet O_2^-$) and hydroxyl radicals ($\bullet OH^-$), *etc.*) [51]. Herein, to better directly identify ROS on TiO_2 and Pd/TiO_2

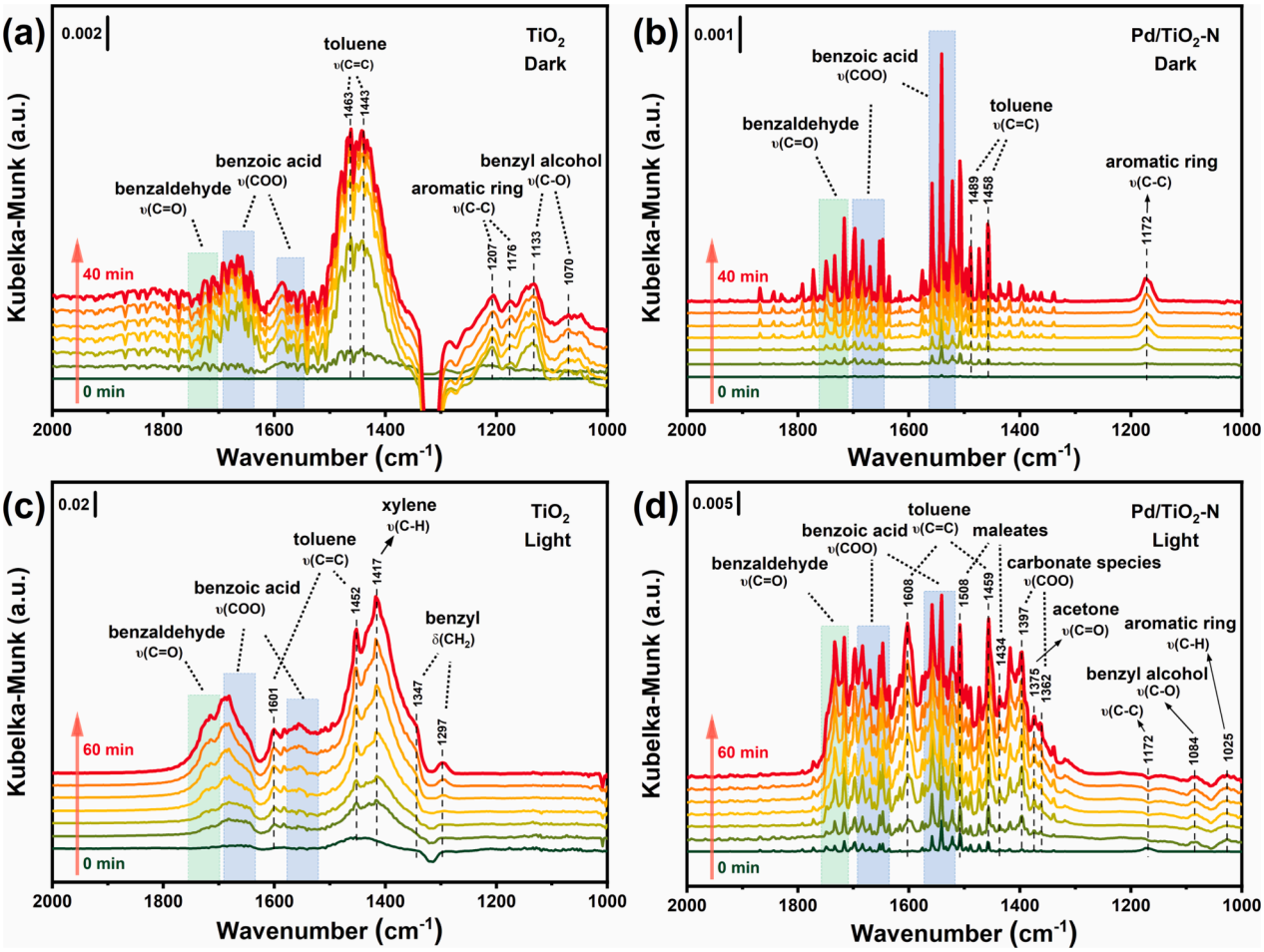

Fig. 7. *In situ* DRIFTS of toluene oxidation on TiO_2 and Pd/TiO_2-N with the light **(a, b)** off and **(c, d)** on.

catalysts, DMPO-ESR trapping experiments were performed. As depicted in Fig. 6c and 6d, both •OH and $\bullet O_2^-$ species were detected on TiO_2 and Pd/TiO_2 catalysts when the light was on, and the intensity of radical signals on Pd/TiO_2-N was much higher than that on Pd/TiO_2-E, Pd/TiO_2-I, and TiO_2, which should be related to the stronger Pd-TiO_2 interaction and higher concentration of surface Ti^{3+}/oxygen defects.

Surface-activated oxygen can reflect the oxygen activation capacity of the catalyst. To further validate this point, O_2-TPD experiments were conducted, as presented in Fig. S6. Broad desorption peaks were observed within the temperature range of 150 to 370 °C for TiO_2, Pd/TiO_2-N, and Pd/TiO_2-E, attributed to the surface chemisorption of oxygen species. In comparison to Pd/TiO_2-E, Pd/TiO_2-N exhibited low-emperature desorption peaks and a larger peak area, indicating an elevated oxygen activation capacity. This difference can be ascribed to the increased presence of surface defects and interactions between the Pd particles and the reducing support in Pd/TiO_2-N. Additionally, two peaks were identified near 450 °C and 558.7 °C, corresponding to subsurface oxygen and lattice oxygen desorption peaks of the samples, respectively [55]. The higher abundance of oxygen defects on the Pd/TiO_2-N surface facilitated the desorption of subsurface oxygen, resulting in elevated desorption peaks.

According to the results of those characterizations above, it was concluded that Pd/TiO_2 catalysts with different surface states (*e.g.*, oxidation states/dispersion of Pd species, concentration of surface Ti^{3+}/oxygen defects, *etc.*) could be tuned by choosing different synthesis routes. Pd/TiO_2-N prepared by one-step reduction of $NaBH_4$ method possessed a relatively higher concentration of Pd^0 species, stronger Pd-TiO_2 interaction and more surface Ti^{3+}/oxygen defects, thus generating narrower band gap width and optimal active species state on Pd/TiO_2-N. The unique photoelectrochemical properties of Pd/TiO_2-N could significantly facilitate the generation of ROS under reaction conditions, enabling its higher toluene conversion and mineralization rate in the photocatalytic oxidation of toluene.

3.5. Mechanism of photocatalytic toluene oxidation

Toluene-TPD experiments were conducted on relevant samples to elucidate the adsorption behavior of toluene and identify key factors influencing the oxidation reaction on catalyst surfaces in varying states. The desorption peak served as an indicator of the toluene adsorption capacity of catalysts. As illustrated in Fig. S7, Pd/TiO_2-N demonstrated a superior toluene adsorption capacity and a lower toluene desorption temperature in comparison to both Pd/TiO_2-E and TiO_2. Among the samples obtained, Pd/TiO_2-N exhibited the highest toluene adsorption capacity, implying that the unique structure resulting from the surface defects of Pd and TiO_2 enhances toluene adsorption capacity.

To deepen the understanding of the structure–activity relationship and the reaction mechanism on the prepared Pd/TiO_2 catalysts in photocatalytic oxidation of toluene, systematic *in situ* DRIFTS experiments were conducted (Fig. S8). For convenience, the attributions of the various IR peaks were summarized and listed in Table S4 according to previous reports [29,56,57]. As shown in Fig. 7 and Fig. S9, with the increase of adsorption time under dark conditions (light source off), unlike that intensive and outstanding bands (*ca.* 1450 cm^{-1}) assigned to the adsorbed toluene were observed on the bare TiO_2, the bands attributed to adsorbed toluene on Pd/TiO_2 catalysts were relatively weaker than those assigned to benzoic acid species, suggesting the more efficient partial oxidation of toluene on Pd/TiO_2 catalysts. Moreover, the

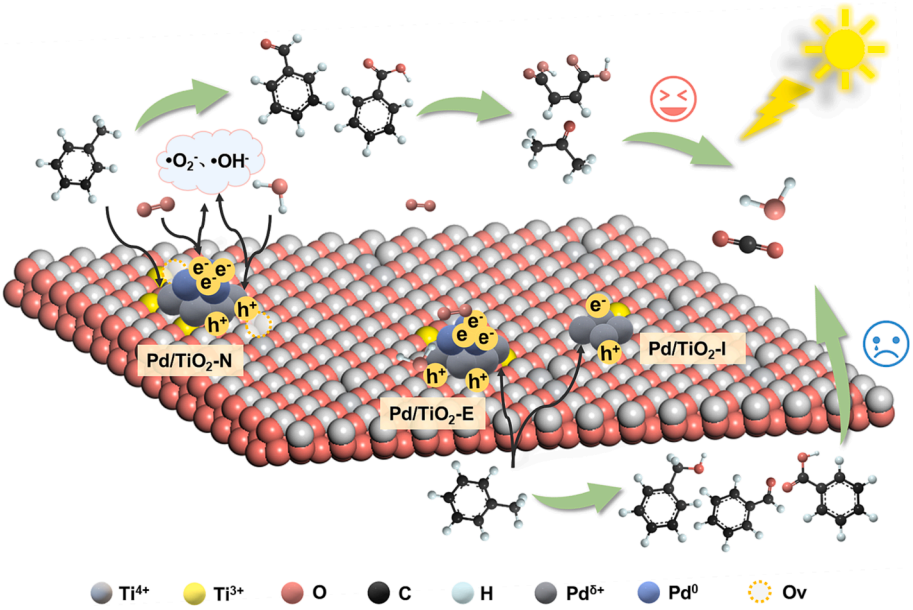

Fig. 8. The reaction pathway of toluene photocatalytic oxidation over Pd/TiO_2 catalysts.

ratio of benzoic species in total aromatic species on Pd/TiO_2-N was much higher than that on Pd/TiO_2-E and Pd/TiO_2-I, which meant that Pd/TiO_2-N could better activate and partially oxidize toluene under dark condition due to a special surface synergistic effect formed by the Pd active clusters as well as their surrounding TiO_2 surface defects. Since benzoic acid species are recognized as the most important intermediates for opening benzene ring in photo-oxidation of toluene [58,59], the advantage of Pd/TiO_2-N in activating and partially oxidizing toluene to benzoic acid species could significantly contribute to its higher activity in photocatalytic oxidation of toluene.

Then, the light source (Xe lamp irradiation) was turned on to further reveal the reaction mechanism of toluene photocatalytic oxidation on TiO_2 and Pd/TiO_2 catalysts. The intensity of bands assigned to various aromatic species on both TiO_2 and Pd/TiO_2 catalysts was enhanced significantly when the light source was turned on, which could be related to the reactive oxygen species (*e.g.*, superoxide radicals ($\bullet O_2^-$) and hydroxyl radicals ($\bullet OH^-$), *etc.*) facilitating the adsorption and activation of toluene. After the light is turned on, the surface reactive oxygen species on the one hand can generate reactive adsorption sites, which interact with toluene molecules through hydrogen bonding, van der Waals forces and other intermolecular interactions. On the other hand, reactive oxygen radicals can introduce unpaired electrons, and when toluene molecules come into contact with the electron-rich sites generated by ROS on the catalyst surface, electron transfer occurs, which leads to the adsorption of toluene molecules onto the catalyst surface [60]. Moreover, the specific types of intermediates also varied greatly on different catalysts. Specifically, for bare TiO_2 and Pd/TiO_2-I, the bands assigned to toluene and xylene species were much more intensive than those bands assigned to partially oxidized aromatic species (*i.e.*, benzyl alcohol, benzaldehyde and benzoic acid, *etc.*). However, for Pd/TiO_2-E and Pd/TiO_2-N, a higher percentage of aromatic species were in the form of benzyl alcohol, benzaldehyde and benzoic acid species. Besides, abundant maleates, carbonate and acetone species were also observed on Pd/TiO_2-E and Pd/TiO_2-N, indicating that toluene could be better activated and oxidized by metallic Pd particles supported on defect-rich TiO_2. Furthermore, a mass of benzaldehyde species accumulated on Pd/TiO_2-E, which was not observed on Pd/TiO_2-N, suggesting that the inefficient deep oxidation of benzaldehyde to benzoic acid or short-chain products possibly resulted from the relatively lower concentration of surface oxygen defects on Pd/TiO_2-E could be one of the main reasons for the relatively lower activity on Pd/TiO_2-E than Pd/TiO_2-N. The accumulation of carbonaceous intermediates without further mineralization on TiO_2, Pd/TiO_2-I and Pd/TiO_2-E could also result in their deactivation, as observed in Fig. 3**a**.

Based on the surface structure of TiO_2 and Pd/TiO_2 as revealed by Raman spectra, XPS, ESR and UV–vis DRS spectra, *etc.*, and the result of *in situ* DRIFTS study, it could be concluded that Pd particles with a higher ratio of Pd^0 species and more surface oxygen defects on Pd/TiO_2-N could better activate toluene and generate ROS under light irradiation, thus effectively promoting the photocatalytic oxidation of toluene. The photocatalytic oxidation of toluene over Pd/TiO_2-N catalyst mainly followed a process of toluene → benzyl alcohol → benzaldehyde → benzoic acid → maleate, short chain carboxylate and aldehyde/ketone (acetone) → CO_2 and H_2O, as shown in Fig. 8.

4. Conclusions

In this work, serial Pd/TiO_2 catalysts with fine-tuned surface structures were synthesized by varied methods and applied for the photocatalytic of toluene. Among those Pd/TiO_2 catalysts, Pd/TiO_2-N with a relatively higher concentration of Pd^0 on Pd particles, richest surface Ti^{3+}/oxygen defects and strongest Pd-TiO_2 interaction showed the most negative VBM, effectively hindered electron-hole complexation and generated the highest concentration of ROS under light irradiation, thus exhibiting much higher toluene conversion and mineralization rate than Pd/TiO_2-E and Pd/TiO_2-I. The stepwise oxidation and ring-opening processes of toluene on Pd/TiO_2 catalysts were also found to be highly sensitive to the surface structure of Pd/TiO_2 catalysts. Specifically, Pd^0 sites on Pd particles could facilitate the partial oxidation of toluene to benzyl alcohol/benzaldehyde/benzoic acid, while surface Ti^{3+}/oxygen defects would induce the ring-opening steps efficiently. This work deeply revealed the reaction mechanism of photocatalytic oxidation of toluene on Pd/TiO_2 catalysts and provided profound insights into constructing efficient photocatalysts to realize the elimination of indoor VOCs under mild conditions.

Declaration of Competing Interest

The authors declare that they have no known competing financial interests or personal relationships that could have appeared to influence the work reported in this paper.

Data availability

Data will be made available on request.

Acknowledgment

This work was supported by financial support from the National Natural Science Foundation of China (21976082, 22106067).

Appendix A. Supplementary data

Supplementary data to this article can be found online at https://doi.org/10.1016/j.cej.2023.146294.

References

[1] N. Li, Q. Jiang, F. Wang, J. Xie, Y. Li, J. Li, S. Wu, Emission behavior, environmental impact and priority-controlled pollutants assessment of volatile organic compounds (VOCs) during asphalt pavement construction based on laboratory experiment, J. Hazard. Mater. 398 (2020), 122904.
[2] P. Yu, N. Li, W. Zou, X. Wei, J. Ji, L. Han, Y. Cai, W. Tan, B. Gao, L. Dong, K+ and CeO2 nanoparticles modified OMS-2 nanorods for enhanced activity and stability of photocatalytic toluene oxidation: K+ charge modulation and mechanistic investigation, Chem. Eng. J. 451 (2023), 138943.
[3] X. Zhou, X. Zhou, C. Wang, H. Zhou, Environmental and human health impacts of volatile organic compounds: a perspective review, Chemosphere 313 (2023), 137489.
[4] K.-T. Han, Effects of Radermachera hainanensis Merr. on air characteristics: a 9-month study in a room with four replications, Build. Environ. 242 (2023), 110496.
[5] Y. Zhang, Y. Wang, R. Xie, H. Huang, M.K.H. Leung, J. Li, D.Y.C. Leung, Photocatalytic oxidation for volatile organic compounds elimination: from fundamental research to practical applications, Environ. Sci. Tech. 56 (2022) 16582–16601.
[6] Z. Zhang, Z. Jiang, W. Shangguan, Low-temperature catalysis for VOCs removal in technology and application: a state-of-the-art review, Catal. Today 264 (2016) 270–278.
[7] H. Sui, P. An, X. Li, S. Cong, L. He, Removal and recovery of o-xylene by silica gel using vacuum swing adsorption, Chem. Eng. J. 316 (2017) 232–242.
[8] K. Li, H. Wang, J. Li, F. Dong, Design and mechanism of photocatalytic oxidation for the removal of air pollutants: a review, Environ. Chem. Lett. 20 (2022) 2687–2708.
[9] X. Wu, R. Han, Q. Liu, Y. Su, S. Lu, L. Yang, C. Song, N. Ji, D. Ma, X. Lu, A review of confined-structure catalysts in the catalytic oxidation of VOCs: synthesis, characterization, and applications, Catalysis Sci. Technol. 11 (2021) 5374–5387.
[10] W. He, X. Zhang, K. Zheng, C. Wu, Y. Pan, H. Li, L. Xu, R. Xu, W. Chen, Y. Liu, C. Wang, Z. Sun, S. Wei, structural evolution of anatase-supported platinum nanoclusters into a platinum-titanium intermetallic containing platinum single atoms for enhanced catalytic CO oxidation, Angew. Chem. Int. Ed. 135 (2023), e202213365.
[11] Y. Lu, Y.P. Zang, H.M. Zhang, Y.X. Zhang, G.Z. Wang, H.J. Zhao, Meaningful comparison of photocatalytic properties of 001 and 101 faceted anatase TiO2 nanocrystals, Science Bulletin 61 (2016) 1003–1012.
[12] A. Migani, L. Blancafort, Excitonic interfacial proton-coupled electron transfer mechanism in the photocatalytic oxidation of methanol to formaldehyde on TiO2 (110), J. Am. Chem. Soc. 138 (2016) 16165–16173.
[13] H. Einaga, K. Mochiduki, Y. Teraoka, Photocatalytic oxidation processes for toluene oxidation over TiO_2 catalysts, Catalysts 3 (2013) 219–231.
[14] Z. Rao, G. Lu, L. Chen, A. Mahmood, G. Shi, Z. Tang, X. Xie, J. Sun, Photocatalytic oxidation mechanism of gas-phase VOCs: unveiling the role of holes, •OH and $•O_2^-$, Chem. Eng. J. 430 (2022), 132766.
[15] J. Ji, Y. Xu, H.B. Huang, M. He, S.L. Liu, G.Y. Liu, R.J. Xie, Q.Y. Feng, Y.J. Shu, Y. J. Zhan, R.M. Fang, X.G. Ye, D.Y.C. Leung, Mesoporous TiO_2 under VUV irradiation: enhanced photocatalytic oxidation for VOCs degradation at room temperature, Chem. Eng. J. 327 (2017) 490–499.
[16] V. Puddu, H. Choi, D.D. Dionysiou, G.L. Puma, TiO_2 photocatalyst for indoor air remediation: influence of crystallinity, crystal phase, and UV radiation intensity on trichloroethylene degradation, Appl Catal B 94 (2010) 211–218.
[17] T.D. Bui, A. Kimura, S. Ikeda, M. Matsumura, Determination of oxygen sources for oxidation of benzene on TiO_2 photocatalysts in aqueous solutions containing molecular oxygen, J. Am. Chem. Soc. 132 (2010) 8453–8458.
[18] A. Naldoni, M. Allieta, S. Santangelo, M. Marelli, F. Fabbri, S. Cappelli, C. L. Bianchi, R. Psaro, V. Dal Santo, Effect of nature and location of defects on bandgap narrowing in black TiO_2 nanoparticles, J. Am. Chem. Soc. 134 (2012) 7600–7603.
[19] L. Nie, B. Duan, A. Lu, L. Zhang, Pd/TiO_2 @ carbon microspheres derived from chitin for highly efficient photocatalytic degradation of volatile organic compounds, ACS Sustain. Chem. Eng. 7 (2019) 1658–1666.
[20] H. Chaker, S. Fourmentin, L. Chérif-Aouali, Efficient photocatalytic degradation of ibuprofen under visible light irradiation using silver and cerium Co-doped mesoporous TiO_2, ChemistrySelect 5 (2020) 11787–11796.
[21] H. Li, Z. Bian, J. Zhu, Y. Huo, H. Li, Y. Lu, Mesoporous Au/TiO_2 nanocomposites with enhanced photocatalytic activity, J. Am. Chem. Soc. 129 (2007) 4538–4539.
[22] C.M. Wang, A. Heller, H. Gerischer, Palladium catalysis of O_2 reduction by electrons accumulated on TiO_2 particles during photoassisted oxidation of organic compounds, J. Am. Chem. Soc. 114 (1992) 5230–5234.
[23] H. Tang, Y. Su, B. Zhang, A.F. Lee, M.A. Isaacs, K. Wilson, L. Li, Y. Ren, J. Huang, M. Haruta, B. Qiao, X. Liu, C. Jin, D. Su, J. Wang, T. Zhang, Classical strong metal-support interactions between gold nanoparticles and titanium dioxide, Sci. Adv. 3 (2017) 1700231.
[24] L. Yan, Q. Wang, W. Qu, T. Yan, H. Li, P. Wang, D. Zhang, Tuning Tiδ+-Vo··-Ptδ+ interfaces over Pt/TiO2 catalysts for efficient photocatalytic oxidation of toluene, Chem. Eng. J. 431 (2022), 134209.
[25] D. Selishchev, D. Svintsitskiy, L. Kovtunova, E. Gerasimov, A. Gladky, D. Kozlov, Surface modification of TiO_2 with Pd nanoparticles for enhanced photocatalytic oxidation of benzene micropollutants, Colloids Surf A Physicochem Eng Asp 612 (2021), 125959.
[26] Q. Wu, J. Ye, W. Qiao, Y. Li, J.W. Niemantsverdriet, E. Richards, F. Pan, R. Su, Inhibit the formation of toxic methylphenolic by-products in photo-decomposition of formaldehyde–toluene/xylene mixtures by Pd cocatalyst on TiO_2, Appl Catal B 291 (2021), 120118.
[27] J.B. Zhong, Y. Lu, W.D. Jiang, Q.M. Meng, X.Y. He, J.Z. Li, Y.Q. Chen, Characterization and photocatalytic property of Pd/TiO_2 with the oxidation of gaseous benzene, J. Hazard. Mater. 168 (2009) 1632–1635.
[28] H. Ma, X. Wang, R. Jin, T. Tan, X. Zhou, R. Fang, Y. Shen, F. Dong, Y. Sun, Promote hydroxyl radical and key intermediates formation for deep toluene mineralization via unique electron transfer channel, J. Colloid Interface Sci. 630 (2023) 704–713.
[29] X. Wei, K. Li, X. Zhang, Q. Tong, J. Ji, Y. Cai, B. Gao, W. Zou, L. Dong, CeO_2 nanosheets with anion-induced oxygen vacancies for promoting photocatalytic toluene mineralization: Toluene adsorption and reactive oxygen species, Appl Catal B 317 (2022), 121694.
[30] M.M. Khan, S.A. Ansari, D. Pradhan, D.H. Han, J. Lee, M.H. Cho, Defect-induced band gap narrowed CeO_2 nanostructures for visible light activities, Ind. Eng. Chem. Res. 53 (2014) 9754–9763.
[31] L. Wang, Y. Cai, B. Liu, L. Dong, A facile synthesis of brown anatase TiO_2 rich in oxygen vacancies and its visible light photocatalytic property, Solid State Ion. 361 (2021), 115564.
[32] J. Qu, Y. Wang, X. Mu, J. Hu, B. Zeng, Y. Lu, M. Sui, R. Li, C. Li, Determination of crystallographic orientation and exposed facets of titanium oxide nanocrystals, Adv. Mater. 34 (2022), 2203320.
[33] Z. Wang, D. Ren, Y. He, M. Hong, Y. Bai, A. Jia, X. Liu, C. Tang, P. Gong, X. Liu, W. Huang, Z. Zhang, Tailoring electronic properties and atom utilizations of the Pd species supported on anatase TiO2{101} for efficient CO2 hydrogenation to formic acid, ACS Catal. 13 (2023) 10056–10064.
[34] C. He, J. Li, X. Zhang, L. Yin, J. Chen, S. Gao, Highly active Pd-based catalysts with hierarchical pore structure for toluene oxidation: catalyst property and reaction determining factor, Chem. Eng. J. 180 (2012) 46–56.
[35] Y. Yang, G. Wang, P. Zheng, F. Dang, J. Han, Carbon deposits during catalytic combustion of toluene on Pd–Pt-based catalysts, Catal. Sci. Technol. 10 (2020) 2452–2461.
[36] Y.Q. Cao, Z.J. Sui, Y. Zhu, X.G. Zhou, D. Chen, Selective hydrogenation of acetylene over Pd-In/Al_2O_3 catalyst: promotional effect of indium and composition-dependent performance, ACS Catal. 7 (2017) 7835–7846.
[37] H. Jeong, J. Bae, J.W. Han, H. Lee, Promoting effects of hydrothermal treatment on the activity and durability of Pd/CeO_2 catalysts for CO oxidation, ACS Catal. 7 (2017) 7097–7105.
[38] N. Della Ca`, M. Fontana, E. Motti, M. Catellani, Pd/Norbornene: a winning combination for selective aromatic functionalization via C-H bond activation, Acc. Chem. Res. 49 (2016) 1389–1400.
[39] Z. Li, X. Dong, M. Zhang, L. Leng, W. Chen, J.H. Horton, J. Wang, Z. Li, W. Wu, Selective hydrogenation on a highly active single-atom catalyst of palladium dispersed on ceria nanorods by defect engineering, ACS Appl. Mater. Interfaces 12 (2020) 57569–57577.
[40] Z. Zhan, H. Wang, Q. Huang, S. Li, X. Yi, Q. Tang, J. Wang, B. Tan, Grafting hypercrosslinked polymers on TiO_2 surface for anchoring ultrafine Pd nanoparticles: Dramatically enhanced efficiency and selectivity toward photocatalytic reduction of CO_2 to CH_4, Small 18 (2022), 2105083.
[41] T. Wang, X. Tao, X. Li, K. Zhang, S. Liu, B. Li, Synergistic Pd single atoms, clusters, and oxygen vacancies on TiO_2 for photocatalytic hydrogen evolution coupled with selective organic oxidation, Small 17 (2021), 2006255.
[42] A. Malankowska, A. Mikolajczyk, J. Medrzycka, I. Wysocka, G. Nowaczyk, M. Jarek, T. Puzyn, E. Mulkiewicz, The effect of Ag, Au, Pt, and Pd on the surface properties, photocatalytic activity and toxicity of multicomponent TiO_2-based nanomaterials, Environmental Science-Nano 7 (2020) 3557–3574.
[43] X. Pan, Y.-J. Xu, Defect-mediated growth of noble-metal (Ag, Pt, and Pd) nanoparticles on TiO2 with oxygen vacancies for photocatalytic redox reactions under visible light, J. Phys. Chem. C 117 (2013) 17996–18005.
[44] X. Chen, L. Liu, P.Y. Yu, S.S. Mao, Increasing solar absorption for photocatalysis with black hydrogenated titanium dioxide nanocrystals, Science 331 (2011) 746–750.
[45] C. Lettmann, K. Hildenbrand, H. Kisch, W. Macyk, W.F. Maier, Visible light photodegradation of 4-chlorophenol with a coke-containing titanium dioxide photocatalyst, Appl Catal B 32 (2001) 215–227.
[46] Z. Sheng, Z. Wu, Y. Liu, H. Wang, Gas-phase photocatalytic oxidation of NO over palladium modified TiO_2 catalysts, Catal. Commun. 9 (2008) 1941–1944.

[47] Z. Wu, Z. Sheng, Y. Liu, H. Wang, N. Tang, J. Wang, Characterization and activity of Pd-modified TiO_2 catalysts for photocatalytic oxidation of NO in gas phase, J. Hazard. Mater. 164 (2009) 542–548.
[48] T.V.M. Sreekanth, P.C. Nagajyothi, G.R. Dillip, Y.R. Lee, Determination of band alignment in the synergistic catalyst of electronic structure-modified graphitic carbon nitride-integrated ceria quantum-dot heterojunctions for rapid degradation of organic pollutants, J. Phys. Chem. C 121 (2017) 25229–25242.
[49] L.Q. Jing, Y.C. Qu, B.Q. Wang, S.D. Li, B.J. Jiang, L.B. Yang, W. Fu, H.G. Fu, J. Z. Sun, Review of photoluminescence performance of nano-sized semiconductor materials and its relationships with photocatalytic activity, Sol Energ Mat Sol C 90 (2006) 1773–1787.
[50] L. Pan, S.B. Wang, J.W. Xie, L. Wang, X.W. Zhang, J.J. Zou, Constructing TiO_2 p-n homojunction for photoelectrochemical and photocatalytic hydrogen generation, Nano Energy 28 (2016) 296–303.
[51] M. Zheng, J. Yang, W. Fan, X. Zhao, Oxygen vacancy and nitrogen doping collaboratively boost performance and stability of TiO_2-supported Pd catalysts for CO_2 photoreduction: a DFT study, PCCP 23 (2021) 24801–24813.
[52] H. Khan, I.K. Swati, Fe3+-doped anatase TiO2 with d-d transition, oxygen vacancies and Ti3+ centers: Synthesis, characterization, UV-vis photocatalytic and mechanistic studies, Ind. Eng. Chem. Res. 55 (2016) 6619–6633.
[53] X.Y. Xin, T. Xu, J. Yin, L. Wang, C.Y. Wang, Management on the location and concentration of Ti3+ in anatase TiO2 for defects-induced visible-light photocatalysis, Appl Catal B 176 (2015) 354–362.
[54] T. Zhang, Y. Chen, X. Yang, J. Chen, J. Zhong, J. Li, M. Li, Z. Wan, Enhanced photocatalytic detoxication properties of OVs-rich Pd/N–TiO_2 heterojunctions: excellent charge separation and mechanism insight, Mater. Today Chem. 28 (2023), 101358.
[55] M. He, Y. Cao, J. Ji, K. Li, H. Huang, Superior catalytic performance of Pd-loaded oxygen-vacancy-rich TiO_2 for formaldehyde oxidation at room temperature, J. Catal. 396 (2021) 122–135.
[56] S. Mo, Q. Zhang, J. Li, Y. Sun, Q. Ren, S. Zou, Q. Zhang, J. Lu, M. Fu, D. Mo, J. Wu, H. Huang, D. Ye, Highly efficient mesoporous MnO_2 catalysts for the total toluene oxidation: oxygen-vacancy defect engineering and involved intermediates using in situ DRIFTS, Appl Catal B 264 (2020), 118464.
[57] S. Huang, C. Zhang, H. He, Complete oxidation of o-xylene over Pd/Al_2O_3 catalyst at low temperature, Catal. Today 139 (2008) 15–23.
[58] P. Chen, W. Cui, H. Wang, X.A. Dong, J. Li, Y. Sun, Y. Zhou, Y. Zhang, F. Dong, The importance of intermediates ring-opening in preventing photocatalyst deactivation during toluene decomposition, Appl Catal B 272 (2020), 118977.
[59] X. Dong, W. Cui, H. Wang, J. Li, Y. Sun, H. Wang, Y. Zhang, H. Huang, F. Dong, Promoting ring-opening efficiency for suppressing toxic intermediates during photocatalytic toluene degradation via surface oxygen vacancies, Science Bulletin 64 (2019) 669–678.
[60] S. Song, S. Zhang, X. Zhang, P. Verma, M. Wen, Advances in catalytic oxidation of volatile organic compounds over Pd-supported catalysts: recent trends and challenges, Front. Mater. 7 (2020), 595667.